NUMERICAL SIMULATION OF PULVERIZED COAL COMBUSTION IN A ROTARY KILN UNDER O_2/CO_2 ATMOSPHERE

by

Guangya WANG, Yifei HUANG, and Hongtao KAO*

College of Materials Science and Engineering, Nanjing Tech University, Nanjing, China

Original scientific paper
https://doi.org/10.2298/TSCI230205126W

The cement industry is the second largest source of global man-made CO_2 emissions after the power industry, and the adoption of O_2/CO_2 combustion technology for cement kilns is of great significance in reducing CO_2 emissions. In this paper, the effects of pulverized coal mixed air combustion and pulverized coal mixed O_2/CO_2 combustion on the velocity field, temperature field, CO_2 and NO_x concentration distribution in rotary kiln were investigated by CFD technique. The results showed that there is no difference in the velocity distribution between the two atmospheres, and the speed difference between the primary and secondary air creates a re-circulation zone near the burner. The O_2/CO_2 atmosphere combustion decreased the maximum temperature, but improved the uniformity of the temperature field. The pulverized coal burnout rate under O_2/CO_2 atmosphere decreased by 3.55% compared to O_2/N_2 atmosphere. The mole fraction of CO_2 at the rotary kiln outlet is 0.08 and 0.93 for O_2/N_2 and O_2/CO_2 combustion atmospheres, respectively. It is easier to achieve CO_2 aggregation and capture under O_2/CO_2 atmosphere than under O_2/N_2. The NO_x concentration at O_2/CO_2 is approximately one half of that at O_2/N_2, which can save the investment on denitrification equipment. The simulation results reasonably agree with the measured data. The findings of this work will provide a reference for the generalization and application of the O_2/CO_2 flue gas cycle calcinating cement technology.

Key words: *cement rotary kiln, O_2/CO_2 combustion, CO_2 emission reduction, numerical simulation*

Introduction

The CO_2 and NO_x are important contributors to the global greenhouse effect, and the cement industry is the second-largest source of CO_2 and NO_x emissions after the power industry [1] Thus, it is an inevitable requirement for the sustainable development of the cement industry to reduce CO_2 and NO_x emissions in cement production.

The O_2/CO_2 combustion technology used in cement rotary kilns involves separating O_2 from the air, combining it with CO_2-rich circulating exhaust gas, and then using this mixture to cool the clinker and produce high temperature O_2/CO_2 gas in the grate cooler. The high temperature gas is sent to the rotary kiln as secondary air for pulverized coal combustion, thereby generating an O_2/CO_2 atmosphere in the kiln. The flue gas is relatively pure CO_2 at the outlet, and the gas can be directly captured and recovered [2] O_2/CO_2 oxygen-enriched combustion technology can simultaneously reduce NO_x, CO_2, and other pollutants, and is an environmentally friendly combustion method.

* Corresponding author, e-mail: kaoht@163.com

A major number of experimental studies on the combustion characteristics of pulverized coal under O_2/CO_2 atmosphere have been carried out. Liu *et al*. [3] found that the factors affecting the reaction characteristics of coal coke in O_2/CO_2 atmosphere were the pyrolysis time and temperature. Kabir and Madugu [4] used appropriate sampling techniques to evaluate the air pollutants in the atmosphere around the cement plant and surrounding settlements and reasonable suggestions for the reduction of pollutant emissions were proposed. Chen *et al*. [5] tested the NO_x emission characteristics during the pulverized coal combustion process in the one-dimension drop tube under O_2/CO_2 and O_2/N_2 atmospheres, and investigated the effects of residence time, fuel/oxygen stoichiometric ratio and temperature on NO_x emission. Suda *et al*. [6] experimentally found that the propagation speed of the combustion flame of pulverized coal in an air atmosphere is faster than that in an O_2/CO_2 atmosphere, but the reasons are not analyzed deeply enough. Li *et al*. [7] found that the ignition temperature and combustion temperature of pulverized coal in the air atmosphere is lower than those in O_2/CO_2 atmosphere in their research tests. Chui *et al*. [8] used CFD to simulate the oxygen-rich combustion characteristics of sub-bituminous coal and obtained that the CO_2 concentration in the flue gas increased. Granados *et al*. [9] simulated the 3-D process of oxygen-enriched combustion of pulverized coal and found that an increase in oxygen concentration would make the flame length of combustion shorter and the radiant heat efficiency would increase substantially. Ditaranto and Bakken [10] demonstrated through simulation that the rotary kiln burner without any modification is suitable for oxyfuel combustion, however, the model assumptions in the study are too ideal.

From the aforementioned research, it can be concluded that O_2/CO_2 combustion technology has been gradually applied in power plant boilers, however, there are few studies on the use of O_2/CO_2 combustion technology in cement production-lines [11, 12], and most of them are concentrated on the decomposing furnace. Considering the importance of cement production reduce CO_2 emissions, this study focuses on the analysis of the possibility of using O_2/CO_2 combustion for rotary kilns.

Since CFD methodology is the mature and low cost [13, 14], this paper takes the rotary kiln of a 2500 tonne per day cement plant in China as the research object and uses ANSYS Fluent 2020R2 software to conduct numerical simulation research of pulverized coal combustion under O_2/CO_2 and O_2/N_2 atmosphere, temperature field, component concentration field distribution was obtained. The results provide a reference for the application of O_2/CO_2 combustion technology in the cement production.

Numerical model

The flow field is solved using the continuity equation, the momentum conservation equation and the energy conservation equation. In pulverized coal combustion using the vortex dissipation model, the gas-phase turbulence model uses the RNG k-ε [15]. The discrete phase model was chosen for gas-solid two-phase flow [16, 17], and the P1 radiation model was used for radiation heat transfer [18, 19].

Basic control equations

The mathematical expression of the continuity equation:

$$\frac{\partial \rho}{\partial \mathrm{t}} + \frac{\partial (\rho u)}{\partial x} + \frac{\partial (\rho v)}{\partial y} + \frac{\partial (\rho w)}{\partial z} = 0 \tag{1}$$

where t is the time variable, ρ – the fluid density, and u, v, and w the vectors of velocity in the x-, y-, and z-directions.

For the conservation of momentum equation, in the present study, it was assumed that the fluid-flows at a steady-state, and the velocity does not change with time. The momentum conservation equation can be expressed as the rate of change of fluid momentum in the micro-element within the fluid should be equal to the sum of the forces that act on the micro-element:

$$\rho\frac{\partial v_i}{\partial t}+\rho v_i\frac{\partial v_i}{\partial x_i}=\rho F_i-\frac{\partial P}{\partial x_i}+\mu\frac{\partial^2 v_j}{\partial x_j^2}+\frac{1}{3}\frac{\partial}{\partial x_i}\left(\frac{\partial v_k}{\partial x_k}\right) \tag{2}$$

where P is the pressure on the micro-element, μ – the viscosity coefficient, v – the velocity vector, v_i, v_j, v_k are velocity vectors in each co-ordinate direction, respectively, and F_i – is the force that act on the micro-element.

In the conservation of momentum equation, the rate of change of the thermodynamic energy of the micro-element within the fluid should be equal to the sum of the heat flux of the micro-element and the work performed on the micro-element by surface forces:

$$\frac{\partial}{\partial x_i}\left(\rho v_i h\right)=\frac{\partial}{\partial x_i}\left(\Gamma_h\frac{\partial h}{\partial x_i}\right)+S_h \tag{3}$$

where $\partial/\partial x_i$ is the convective transport of enthalpy within the cell grid, $\partial/\partial x$ – the diffusion and transport of enthalpy within the cell grid, $\Gamma_h(\partial h/\partial x_i)$ – the source of enthalpy, and S_h – is the source term for coal combustion and radiation heat.

The pulverized coal combustion model

The process of pulverized coal combustion can be divided into the combustion of volatile matter and the combustion of coke [20]. In the present study, the single-rate reaction model was used to calculate the combustion of volatile matter. The diffusion-limited reaction model was used to calculate the combustion of coke. The single-rate reaction model assumes that the volatilization rate is the first-order, and that the volatilization rate can be determined by the residual volatiles in the coal particles. The linear function can be expressed:

$$\frac{\mathrm{d}m_p}{\mathrm{d}t}=-k\left[m_p-\left(1-f_{u,0}\right)\left(1-f_{v,0}\right)m_{p,0}\right] \tag{4}$$

$$k=A\mathrm{e}^{-(E/\mathrm{R}T)} \tag{5}$$

where m_p is the particle mass, $m_{p,0}$ – the initial particle mass, k – the kinetic parameter, $f_{u,0}$ – the mass fraction of volatile matter in the initial particle, $f_{v,0}$ – the mass fraction of volatile matter, A – the pre-exponential factor, E – the activation energy of the reaction, and R – the gas constant.

The diffusion-limited reaction model assumes that the combustion rate of coke depends on the diffusion rate. The coke rate model:

$$\frac{\mathrm{d}m_p}{\mathrm{d}t}=-A_\alpha P_{\beta x}\frac{D_0 k}{D_0+k} \tag{6}$$

where A_α is the remaining area of coke, $P_{\beta x}$ – the atmospheric pressure around the granule, D_0 – the diffusion coefficient that covers the granule surface, and k – the kinetic rate.

The NO_x generation model

The nitric oxide produced by the combustion of pulverized coal mainly includes thermal NO_x, prompt NO_x, and fuel NO_x. During the pulverized coal combustion process in the

rotary kiln, NO is predominantly produced, while the amounts of NO_2 and N_2O account for only 5% of the total NO_x emissions [21]. Therefore, merely NO was considered in the calculation of NO_x. In most pulverized coal combustions, the percentage of prompt NO_x generation is less than 5% [22]. Therefore, in the present study, the prompt NO_x was ignored, and merely thermal NO_x and fuel NO_x were considered. According to the generalized Zeldovich theorem, the thermal NO_x generation mode is [23]:

$$O_2 \leftrightarrow O + O \tag{7}$$

$$O + N_2 \leftrightarrow N + NO \tag{8}$$

$$N + O_2 \leftrightarrow NO + O \tag{9}$$

$$N + OH \leftrightarrow H + NO \tag{10}$$

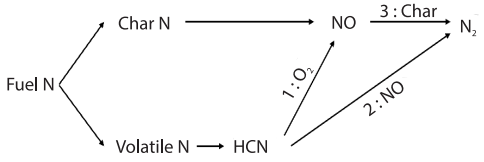

Figure 1. Reaction generation pathway of fuel-based NO_x

The reaction generation pathway of fuel-based NO_x is shown in fig. 1. Assuming that the N in the fuel is concentrated in the fixed carbon and volatiles, the N in the volatiles is first converted into HCN, and part of the HCN reacts with O_2 to generate NO. The HCN that is not involved in the oxidation reaction is mixed with the generated NO, and the HCN at this time acts as a reducing agent to reduce NO to N_2. Since the residual coke N has a certain reducibility, a part of NO can also be directly reduced to N_2.

The physical model and boundary conditions

Based on the data obtained from the thermal calibration of cement, the parameters of the boundary conditions for the numerical simulation are given in tab. 1.

Table 1. Parameters of cement rotary kiln

Parameters	Unit	Specification
Size	[m]	Ø4 × 60 m
Production capacity	[tonne per day]	2500
Slope	[%]	3.5
Rotational Speed	[rpm]	0.396-3.96
Motor power	[kW]	315

The size of the rotary kiln used in this paper is Ø4 × 46 m. Due to the thickness of the refractory bricks, the size of the computational domain of the model is defined as Ø3.6 × 46 m. The computational domain model as shown in fig. 2. In this paper, the rotary kiln adopts the meshing of hexahedral structure, with local encryption near the burner, the number of meshes generated is about 1.48 million, the mesh quality is 0.6, the mesh presents overall tightness, the mesh quality is good, and there is no bad mesh. Figure 3 shows the grid division of the rotary kiln system.

The sensitivity and independence of the grids were analyzed based on the data in fig. 4, and the results showed that the number of grids (1472754 cells) had no effect on the results of this study. The rotary kiln outlet is set as a pressure outlet, all walls are set as insu-

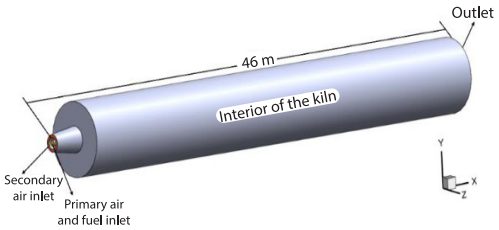

Figure 2. Calculation domain model of rotary kiln

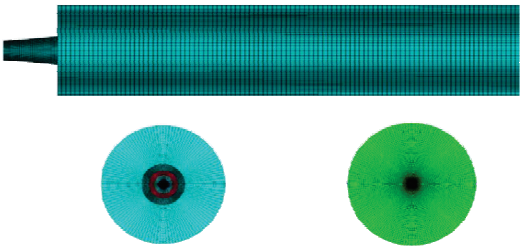

Figure 3. Grid of rotary kiln

lated walls, and all air inlet channels are set as velocity inlets perpendicular to the boundary. The specific boundary conditions are shown in tab. 2. The proximate and ultimate analysis of the coal dust used in this paper is shown in tab. 3, M_{ad} refers to the air-dried coal moisture, A_{ad} refers to the air-dried coal ash, V_{ad} refers to the air-dried coal volatiles, and FC_{ad} refers to the air fixed carbon content. The particle size analysis of the pulverized coal is in accordance with the Rosin-Rampler distribution, and the particle size distribution parameters of the pulverized coal are shown in tab. 4.

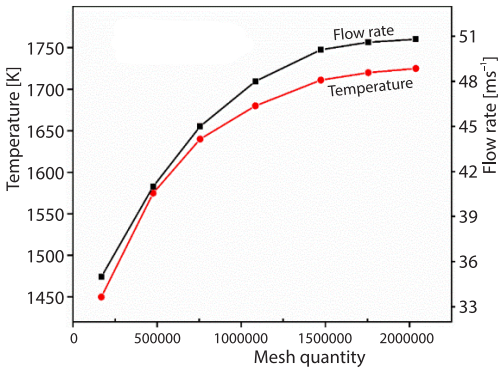

Figure 4. Grid independence verification

Table 2. Boundary conditions

	Primary air inlet	Secondary air inlet	Kiln outlet	Nozzle
Boundary type	Velocity inlet	Velocity inlet	Pressure outlet	Wall
Temperature [K]	300	1500	–	Heat insulation
Velocity [ms^{-1}]	150	40	–	–
Turbulence intensity [%]	4.0	3.3	5.0	–
Ratio [%]	21	79	–	–

Table 3. Proximate and ultimate analysis of pulverized coal

Proximate analysis [%]				Ultimate analysis [%]					$Q_{net,ar}$ [MJkg^{-1}]
M_{ad}	A_{ad}	V_{ad}	FC_{ad}	C_{ar}	H_{ar}	O_{ar}	N_{ar}	S_{ar}	
4.14	23.62	31.68	40.56	40.12	3.2	27.62	1.04	0.26	27.962

Table 4. Particle size distribution parameters of pulverized coal

Particle size type	Rosin-Rammler
Minimum particle size	$1 \cdot 10^{-6}$ m
Maximum particle size	$1.6 \cdot 10^{-4}$ m
Average particle size	$8 \cdot 10^{-5}$ m
Characteristic particle size	50.284 μm
Uniformity index	1.1

Experimental validation

From the data in the tab. 5, it can be seen that the deviation between the simulation and measurement of the kiln tail temperature is 8.3% at most. This is because the numerical simulation is under an ideal condition, but the measured values are based on the average value of the actual operation. In addition, the walls are considered adiabatic, so there is no surface heat loss, which is not possible under practical conditions. The relative error of other parameters is about 5%, all less than 10%, which meets engineering needs. This shows that the model proposed in this work is reliable.

Table 5. Comparison of simulation and experimental data

Parameters	Simulation values	Experimental value	Relative error [%]
Kiln tail temperature [K]	1745	1663	8.3
Kiln tail pressure [Pa]	–80	−268	4.5
Kiln tail CO_2 mole fraction	0.08	0.076	5.3
Kiln tail NO_x concentration [mgm^{-3}]	515	549	-6.2

Results and analysis

Speed field

Replacing N_2 with CO_2 causes a composition change of the air-flow. It is necessary to determine whether this will result in significant changes in the overall flow field. The simulation results indicate that replacing N_2 with CO_2 will not cause any changes to the distribution of velocity field inside the kiln. The velocity vectors under two working conditions are shown in fig. 5. Both atmospheres show a *mallet* shape in the middle part where the speed is higher. This is because the speed of the cyclonic flow in the primary air is much higher than that of the secondary air. Meanwhile, the large speed difference between the swirl air and the secondary air makes the surrounding air-flow form a re-circulation zone, which allows the pulverized coal to prolong the residence time and fully burn. This finding is consistent with Wang's and Huang's research results [24, 25] . The backflow area gradually disappears along the length of the rotary kiln, and then the air-flow is evenly distributed forward, and finally flows out from the outlet.

Figure 6 shows the velocity vector diagrams of the rotary kiln along the $X = 22$ m section in O_2/N_2 atmosphere and O_2/CO_2 atmosphere. The partial enlargement in the fig. 6 clearly shows the state of the reflux area in the kiln. The effect of the cyclone causes the air-flow spread evenly in all directions, which helps to make the residual coke burn out and improves the combustion efficiency of pulverized coal.

Temperature field

Figure 7 shows the temperature contour along the axial section of the rotary kiln. It is easy to determine that a local low temperature region exists near the burner, which is beneficial for protecting the burner from damage. It shows that the two cases had nearly the same flame shape which is consistent with the actual flame shape in production. The flame length in the high temperature region under O_2/CO_2 atmosphere is shorter than that under O_2/N_2 atmosphere, which can be explained by the following factors. On one hand, the specific heat capacity of CO_2 is higher than that of N_2, and CO_2 absorbs more heat than N_2 to lower the fuel temperature, which hinders the efficient diffusion of heat and major fuel components from the reaction zone

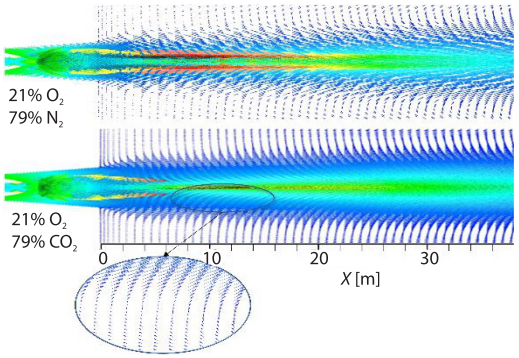

Figure 5. Velocity vector at vertical cross-section through the kiln axis under two working conditions

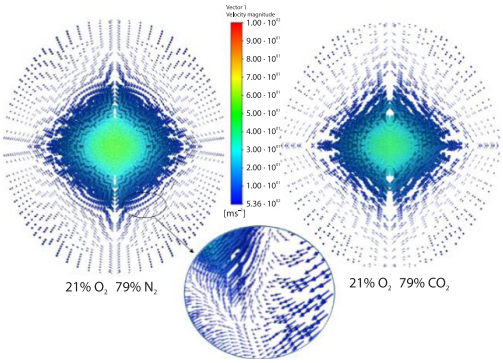

Figure 6. Velocity vector at X = 22 m cross-section under two working conditions

to the preheating zone, and finally reduces the flame length. On the other hand, the low diffusion rate of CO_2 blocks the diffusion of fuel components to the preheating zone, which also reduces the flame length to some extent.

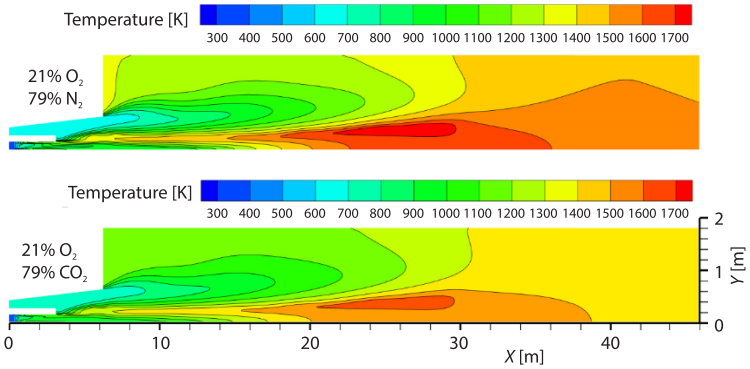

Figure 7. Temperature contours under two working conditions

From tab. 6, it can be seen that the burnout rates of pulverized coal in the atmospheres of O_2/N_2 and O_2/CO_2 are 96.23% and 92.68%, respectively. In comparison, the burnout rates of pulverized coal under the O_2/CO_2 atmosphere decreased by 3.55%, indicating a deterioration in the combustion characteristics of the pulverized coal, which is similar to the results obtained in Xu's research [26].

Table 6. Burnout rate of pulverized coal under different atmospheres

Combustion atmosphere	Pulverized coal burnout rate [%]
O_2/N_2	96.23
O_2/CO_2	92.68

The average and maximum temperatures for the two conditions can be shown in fig. 8. In order to satisfy the calcination of cement clinker, the maximum temperature in the kiln must reach 1600 K, which indicates that O_2/CO_2 atmosphere can satisfy the conditions for calcination of cement clinker. Due to the long length and large size of the rotary kiln, the maxi-

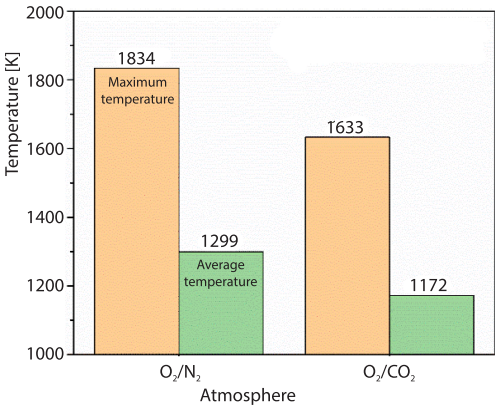

Figure 8. Maximum and average temperature in the kiln under two working conditions

mum temperature in the kiln was quite different from the average temperature under two conditions. Replacing the O_2/N_2 atmosphere with an O_2/CO_2 atmosphere resulted in a decrease in the maximum temperature from 1834-1633 K, and this change can be attributed to its higher specific heat capacity than that of N_2, which means it can absorb more heat energy without significant increase the temperature. This in turn leads to a reduction in the temperature rise of the N_2 as the fuel releases the same amount of heat. However, the kiln's average temperature dropped only slightly, from 1299-1172 K, indicating a more even distribution of temperature throughout the kiln when using an O_2/CO_2 atmosphere.

The CO_2 concentration analysis

Figure 9 shows the molar fraction of CO_2 at the Z = 0 m section along the length direction of the rotary kiln under two combustion atmospheres. It can be seen that in the O_2/N_2 atmosphere, due to the negligible participation of N_2 in combustion reactions, the mole fraction of CO_2 gradually increases from 0-0.08. In the O_2/CO_2 atmosphere, with the initial molar fraction of CO_2 at 79% and the continuous generation of CO_2 during coal combustion, the maximum molar concentration of CO_2 at the outlet of the rotary kiln can reach 93%. This high concentration of CO_2 is more conducive to large-scale capture and centralized treatment, reducing CO_2 emissions in cement production.

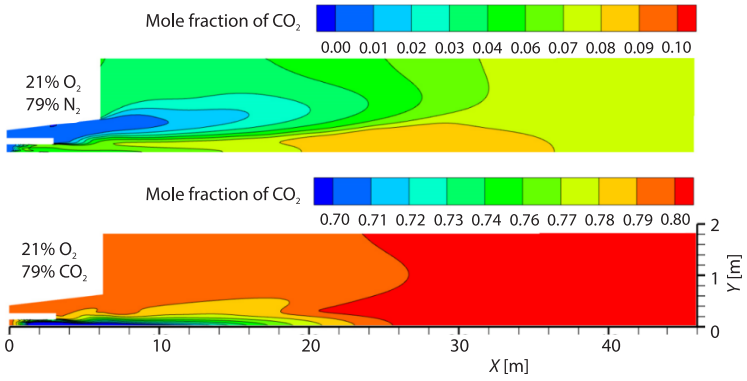

Figure 9. Contours of CO_2 molar fraction in Z = 0 m section under two working conditions

Figure 10 shows the variations in the mole fraction of CO_2 along the central axis of the rotary kiln under two different atmospheres. It can be seen that both conditions exhibit a trend of initially increasing and then stabilizing CO_2 concentration. However, due to different initial mole fractions, the CO_2 mole fractions at the kiln outlet under the O_2/N_2 and O_2/CO_2 combustion atmospheres are 0.08 and 0.93, respectively. Therefore, it is easier to achieve CO2 capture and aggregation using the O_2/CO_2 atmosphere.

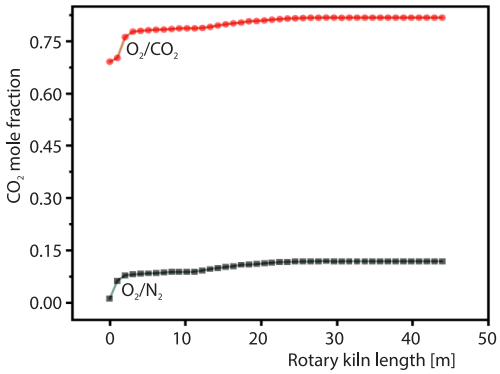

Figure 10. The CO_2 molar fraction along the center axis of the rotary kiln

The NO_x distribution analysis

Figure 11 shows the NO_x distribution in $Z = 0$ m section of rotary kiln under two working conditions. It can be seen that the NO_x generation under O_2/N_2 atmosphere is significantly higher than that under O_2/CO_2 atmosphere, the NO_x concentration in the high temperature area under O_2/N_2 atmosphere has reached 646 mgNm^{-3}, and the average concentration ranges from 430-539 mgN/m^3. In contrast, the NO_x concentration under the O_2/CO_2 atmosphere is maintained at 355 mgN/m^3, which is below the national standard of 400 mgN/m^3. This eliminates the need for the SCR/SNCR post-treatment process, saving investment and operational costs of ammonia injection.

In O_2/N_2 atmosphere and O_2/CO_2 atmosphere, the NO_x along the length of the rotary kiln is shown in fig. 12. The trends of NO_x mole fraction under the two working conditions were basically the same, both showed an initial increase, followed by a decrease, and eventually reaching a stable level. The 15 meters from the kiln head is the high temperature zone generated by the full combustion of pulverized coal. At this location, a significant amount of thermal NO_x is generated inside the rotary kiln, and the concentration reaches the maximum. After the high temperature zone, the nitrogen-containing oxides in the fuel generate a small amount of fuel NO_x, and the NO_x concentration decreases rapidly. In the NO_x generation process of the rotary kiln, the thermal type dominates, therefore, the NO_x concentration distribution follows the temperature distribution in the kiln, which is in line with the thermal type NO_x generation mechanism. However, in the O_2/CO_2 atmosphere, NO_x concentration is reduced since thermal NOx cannot be generated without N_2.

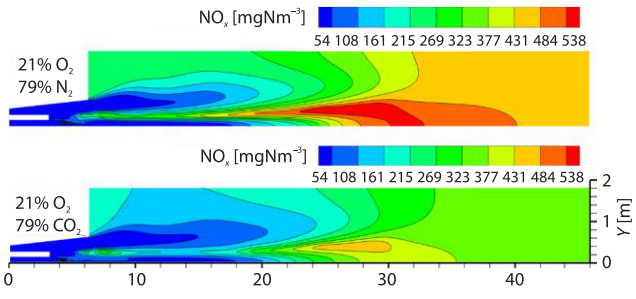

Figure 11. The NO_x distribution at $Z = 0$ m section of rotary kiln under two working conditions

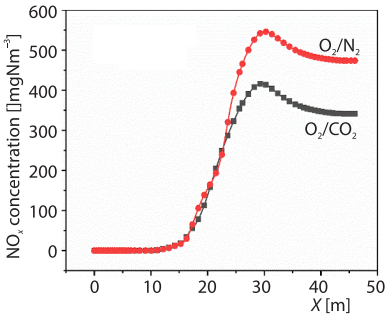

Figure 12. Change of NO_x concentration

Glarborg and Bentzen [27] conducted experimental and simulation studies of the chemical effects of high CO_2 concentrations and concluded that the O_2/CO_2 atmosphere produces higher concentrations of CO compared to the O_2/N_2 atmosphere, which has a positive effect on the reduction of NO_x generation. When the temperature is greater than 1300 K, the rate of reaction (11) will be high, and CO_2 will react with coal coke to produce large amounts of CO. Although coal coke has limited ability to reduce NO_x, at high temperatures, CO exhibits a significant catalytic effect on the reaction between coal coke and NO_x, which makes the reaction (12) faster. Meanwhile, more NO_x is reduced by CO through reaction (13) in the presence of coal coke catalysis:

$$C + CO_2 \rightarrow 2CO \tag{11}$$

$$\text{Char} + NO \rightarrow \frac{1}{2}N_2 + \ldots \tag{12}$$

$$CO + NO \xrightarrow{\text{char}} N_2 + \ldots \tag{13}$$

Combustion in an O_2/CO_2 atmosphere can significantly reduce NO_x emissions mainly for the following reasons:

– Without the involvement of N_2 in the O_2/CO_2 atmosphere, there is no thermodynamic NO_x generation at high temperatures, thus greatly reducing the overall NO_x concentration.
– High concentrations of CO_2 lead to high concentrations of CO allowing NO to be reduced to N_2.
– The temperature of the combustion chamber under O_2/CO_2 atmosphere will be reduced, and at the same time, the NO production will be reduced.

Conclusion

This paper presents a simulation study of pulverized coal combustion in a rotary kiln under two different combustion atmospheres. The speed field, temperature field, and distribution of CO_2 and NO_x inside the kiln are compared and analyzed. The simulation results were validated by experimental results and showed good agreement. The results indicate that there is no difference in the velocity distribution between two atmospheres, and the velocity difference between the primary and secondary air creates a re-circulation zone near the burner. The O_2/CO_2 atmosphere combustion decreased the flame length and maximum temperature, but improved the uniformity of the temperature field in the kiln. The pulverized coal burnout rate under O_2/CO_2 atmosphere decreased by 3.55% compared to O_2/N_2 atmosphere. The CO_2 mole fraction at the rotary kiln outlet is 0.08 and 0.93 for O_2/N_2 and O_2/CO_2 combustion atmospheres, respectively. The NO_x concentration at O_2/CO_2 is approximately one half of that at O_2/N_2, which can save the investment on denitrification equipment. This study provides a theoretical basis for further research on the O_2/CO_2 combustion of the cement kiln.

References

[1] Liu, Y., Kao, H. T., Numerical Simulation of Urea Based SNCR Process in a Trinal-Sprayed Precalciner, *Journal of Renewable Materials*, *9* (2021), 2, pp. 269-294
[2] Zhang, L. Y., *et al*., Numerical Simulation of Oxy-Fuel Combustion with Different O_2/CO fractions in Large Cement Precalciner, *Energy and Fuels*, *34* (2020), 4, pp. 4949-4957
[3] Liu, Y., *et al*., A Study on Coal Combustion and Desulfurizaion Chara Cteristics in Atmosphere Containing O_2/CO_2, *Proceedings of the Chinese Society of Electrical Engineering*, *24* (2004), 8, pp. 224-228
[4] Kabir, G., Madugu, A. I., Assessment of Environmental Impact on Air Quality by Cement Industry and Mitigating Measures: A Case Study, *Environmental Monitoring and Assessment*, *160* (2010), 1-4, pp. 91-99

[5] Chen, C. M., *et al*., Experimental Study on NO_x Emission from Coal Combustion under O_2/CO_2 Atmosphere, *Journal of Southeast University*, *35* (2005), 5, pp. 738-741
[6] Suda, T., *et al*., Effect of Carbon Dioxide on Flame Propagation of Pulverized Coal Clouds in CO_2/O_2 Combustion, *Fuel*, *86* (2007), 12-13, pp. 2008-2015
[7] Li, D. B., *et al*., Coal Combustion Characteristics and Kinetics Analysis in O_2/CO_2 Atmosphere, *Journal of Combustion Science and Technology*, *24* (2018), 3, pp. 223-231
[8] Chui, E., *et al*., Modelling of Oxy-Fuel Combustion for a Western Canadian Sub-Bituminous Coal, *Fuel*, *82* (2003), 10, pp. 1201-1210
[9] Granados, D. A., *et a*l., Effect of Flue Gas Re-Circulation during Oxy-Fuel Combustion in a Rotary Cement Kiln, *Energy*, *64* (2014), Jan., pp. 615-625
[10] Ditaranto, M., Bakken, J., Study of a Full Scale Oxy-Fuel Cement Rotary Kiln, *International Journal of Greenhouse Gas Control*, *83* (2019), Apr., pp. 166-175
[11] Telesca, A., *et al*., Low-CO_2 Cements from Fluidized Bed Process Wastes and Other Industrial By-Products, *Combustion Science and Technology*, *188* (2016), 4-5, pp. 492-503
[12] Granados, D. A., *et al*., Oxy-Fuel Combustion as an Alternative for Increasing Lime Production in Rotary Kilns, *Applied Energy*, *158* (2015), 4, pp. 107-117
[13] Rybdylova, O., *et al*., A model for Droplet Heating and Its Implementation into ANSYS FLUENT, *International Communications in Heat and Mass Transfer*, *76* (2016), Aug., pp. 265-270
[14] Wang, X., *et al*., Prediction of Falling Film Evaporation on the AP1000 Passive Containment Cooling System Using ANSYS FLUENT Code, *Annals of Nuclear Energy*, *95* (2016), Sept., pp. 168-175
[15] Branco, J., *et al.*, Experimental and Numerical Investigation of Turbulent Diffusion Flames in A Laboratory Combustor with a Slot Burner, *Fuel*, *175* (2016), July, pp. 182-190
[16] Rahmanian, B., *et al*., Investigation of Pollutant Reduction by Simulation of Turbulent Non-Premixed Pulverized Coal Combustion, *Applied Thermal Engineering*, *73* (2014), 1, pp. 1222-1235
[17] Gomez, M. A., *et al*., Numerical Simulation of the Combustion Process of a Pellet-Drop-Feed Boiler, *Fuel*, *184* (2016), Nov., pp. 987-999
[18] Mujumdar, K. S., Ranade, V. V., The CFD Modelling of Rotary Cement Kilns, *Asia-Pacific Journal of Chemical Engineering*, *3* (2008), 2, pp. 106-118
[19] Kangwanpongpan, T., *et al*., Prediction of Oxy-Coal Combustion through an Optimized Weighted Sum of Gray Gases Model, *Energy*, *41* (2012), 1, pp. 244-251
[20] Zhu, G., *et al.*, Study on NO_x Emissions during the Coupling Process of Preheating-Combustion of Pulverized Coal with Multi-Air Staging, *Journal of Cleaner Production*, *292* (2021), 126012
[21] Pieper, C., *et al*., Numerical Investigation of the Impact of Coating Layers on RDF Combustion and Clinker Properties in Rotary Cement Kilns, *Fuel*, 283 (2021), 118951
[22] Liu, J., *et al*., Carbon and Air Pollutant Emissions from China's Cement Industry 1990-2015: Trends, Evolution of Technologies, and Drivers, *Atmospheric Chemistry and Physics*, *21* (2021), 3, pp. 1627-1647
[23] Bhunia, S., *et al*., Reaction Kinetics of Coal Char in Oxy-Fuel Combustion Environment and Characterization of Reacted Char, in: *Energy Sources Part a: Recovery Utilization and Environmental Effects*, Taylor & Francis, Oxford, UK, 2021, pp. 1-23
[24] Wang, M., *et al*., Numerical Simulation of Oxy-Coal Combustion in a Rotary Cement Kiln, *Applied Thermal Engineering*, *103* (2016), June, pp. 491-500
[25] Huang, Y., *et al*., Numerical Simulation of Pulverized Coal Combustion in Rotary Kilns with Different Oxygen Concentrations, *Energy Sources Part a-Recovery Utilization and Environmental Effects*, *44* (2022), 2, pp. 4510-4524
[26] S, X. S., *et al*., Numerical Simulation and Reliability Verification of Pulverized Coal Combustion in Rotary Kiln and Decomposing Furnace under O_2/CO_2 Condition, *Chinese Journal of Environmental Engineering*, *14* (2020), 5, pp. 1311-1319
[27] Glarborg, P., Bentzen, L. L. B., Chemical Effects of a High CO_2 Concentration in Oxy-Fuel Combustion of Methane, *Energy and Fuels*, *22* (2008), 1, pp. 291-296

Paper submitted: February 5, 2023
Paper revised: April 20, 2023
Paper accepted: April 27, 2023